In vivo volumetric imaging of subcutaneous microvasculature by photoacoustic microscopy

Hao F. Zhang, Konstantin Maslov, and Meng-Lin Li

Department of Biomedical Engineering, Texas A&M University, College Station, TX 77843

George Stoica

Department of Veterinary Pathobiology, Texas A&M University, College Station, Texas 77843

Lihong V. Wang

Department of Biomedical Engineering, Texas A&M University, College Station, TX 77843
lwang@bme.tamu.edu

Abstract: Photoacoustic microscopy was developed to achieve volumetric imaging of the anatomy and functions of the subcutaneous microvasculature in both small animals and humans *in vivo* with high spatial resolution and high signal-to-background ratio. By following the skin contour in raster scanning, the ultrasonic transducer maintains focusing in the region of interest. Furthermore, off-focus lateral resolution is improved by using a synthetic-aperture focusing technique based on the virtual point detector concept. Structural images are acquired in both rats and humans, whereas functional images representing hemoglobin oxygen saturation are acquired in rats. After multiscale vesselness filtering, arterioles and venules in the image are separated based on the imaged oxygen saturation levels. Detailed structural information, such as vessel depth and spatial orientation, are revealed by volume rendering.

OCIS codes: (170.3880) Medical and biological imaging; (170.5120) Photoacoustic imaging; (180.5810) Scanning microscopy.

References and links

1. R. L. Barnhill, K. Fandrey, M. A. Levy, M. C. Mihm, and B. Hyman, "Angiogenesis and tumor progression of melanoma: quantification of vascularity in melanocytic nevi and cutaneous malignant melanoma," Lab. Invest. **67**, 331-337 (1992).
2. H. Nakajima, T. Minabe, and N. Imanishi, "Three-dimensional analysis and classification of arteries in the skin and subcutaneous adipofascial tissue by computer graphics imaging," Plast. Reconstr. Surg. **102**, 748-760 (1998).
3. X. Wang, Y. Pang, G. Ku, X. Xie, G. Stoica, and L. V. Wang, "Noninvasive laser-induced photoacoustic tomography for structural and functional *in vivo* imaging of the brain," Nat. Biotechnol. **25**, 114-116 (2000).
4. R. R. Edelman, H. P. Mattle, D. J. Atkinson, and H. M. Hoogewoud, "MR angiography," Am. J. Roentgenol. **154**, 937-946 (1990).
5. Y. Zhao, Z. Chen, C. Saxer, S. Xiang, J. F. de Boer, and J. S. Nelson, "Phase-resolved optical coherence tomography and optical Doppler tomography for imaging blood flow in human skin with fast scanning speed and high velocity sensitivity," Opt. Lett. **25**, 114-116 (2000).
6. F. A. Duck, Physical Properties of Tissue (Academic Press, San Diego, CA, 1990).
7. C. G. A. Hoelen, F. F. M. de Mul, R. Pongers, and A. Dekker, "Three-dimensional photoacoustic imaging of blood vessels in tissue," Opt. Lett. **23**, 648-650 (1998).
8. M. C. Pilatou, N. J. Voogd, F. F. M. de Mul, and W. Steenbergen, "Analysis of three-dimensional photoacoustic imaging of a vasculature tree *in vitro*," Rev. Sci. Instrum. **74**, 4495-4499 (2003).
9. R. G. Kolkman, E. Hondebrink, W. Steenbergen, and F. F. M. de Mul, "*In vivo* photoacoustic imaging of blood vessels using an extreme-narrow aperture sensor," IEEE J. Sel. Top. Quantum Electron **9**, 343-346 (2003).
10. X. Wang, Y. Pang, G. Ku, G. Stoica, and L. V. Wang, "Three-dimensional laser-induced photoacoustic tomography of mouse brain with the skin and skull intact," Opt. Lett. **28**, 1739-1741 (2003).
11. M. Xu, and L. V. Wang, "Photoacoustic imaging in biomedicine," Rev. Sci. Instrum. **77**, 041101 (2006).

#72153 - $15.00 USD Received 20 June 2006; revised 14 August 2006; accepted 14 August 2006

12. A. A. Oraevsky, and A. A. Karabutov, "Optoacoustic Tomography," in *Biomedical Photonics Handbook*, T. Vo-Dinh ed. (CRC Press, Boca Raton, FL, 2003).
13. M. Xu, and L. V. Wang, "Analytic explanation of spatial resolution related to bandwidth and detector aperture size in thermoacoustic and photoacoustic reconstruction," Phys. Rev. E **67**, 1-15 (2003).
14. K. Maslov, G. Stoica, and L. V. Wang, "*In vivo* dark-field reflection-mode photoacoustic microscopy," Opt. Lett. **30**, 625-627 (2005).
15. H. F. Zhang, K. Maslov, G. Stoica, and L. V. Wang, "Functional photoacoustic microscopy for high-resolution and noninvasive *in vivo* imaging," Nature Biotechnol. **24**, 848-851 (2006).
16. National Institutes of Health, "Guide for the Care and Use of Laboratory Animals," (U.S. Government Printing Office, Washington DC, 1985), NIH Pub. 86-23.
17. M.-L. Li, H. F. Zhang, K. Maslov, G. Stoica, and L. V. Wang, "Improved in-vivo photoacoustic microscopy based on a virtual detector concept," Opt. Lett. **31**, 474-476 (2006).
18. D. Jensen, *The principles of physiology* (Appleton-Century-Crofts, New York 1976), pp 746.
19. K. Maslov, M. Sivaramakrishnan, H. F. Zhang, G. Stoica, and L. V. Wang, "Technical considerations in quantitative blood oxygenation measurement using photoacoustic microscopy in small animal *in vivo*," in *Photons Plus Ultrasound: Imaging and Sensing 2006*, A. A. Oraevsky and L. V. Wang, eds., Proc. SPIE **6086**, 215-225 (2006).
20. A. F. Frangi, W. J. Niessen, K. L. Vincken, M. A. Viergever, "Multiscale vessel enhancement filtering," in *Proceedings of Medical Image Computing & Computer Assisted Intervention (MICCAI)*, W. Wells, A. Colchester, and S. Delp, eds., Vol. 1496 of Lecture Notes in Computer Science, (Springer-Verlag, Berlin 1998), pp.130-137.
21. American national standard for the safe use of lasers Z136.1, (American National Standards Institute, New York, 2000).
22. P. Carmeliet and R. K. Jain, "Angiogenesis in cancer and other disease," Nature **407**, 249-257 (2000).
23. C. M. van Vemmel, L. J. Spreeuwers, M. A. Viergever, and W. J. Niessen, "Level-set-based artery-vein separation in blood pool agent CE-MR angiograms," IEEE Trans. Med. Imaging. **22**, 1224-1234 (2003).

1. Introduction

High-resolution imaging of subcutaneous blood microvessels in three dimensions can be of great benefit to dermatology, cancer research [1], and plastic surgery [2]. However, accurate noninvasive imaging of the anatomy and functions of the subcutaneous microvasculature remains a challenge. First, the imaging modality employed must have high sensitivity so that small-diameter (tens of μm) blood vessels can be detected. Second, the imaging modality employed must have high spatial resolution so that the vessel network can be resolved. Third, it must have enough penetration depth so that the major vasculature in the dermal layer (1-3 mm below the skin surface in humans and small animals) can be measured. Fourth, it must be able to acquire volumetric data with good spatial resolution in both the lateral and axial directions. Fifth, it must image appropriate intrinsic contrast so that physiological functions can be measured.

In blood vessel imaging, the intrinsic contrast comes from either the strong optical absorption of hemoglobin [3] or the velocity of the blood flow [4,5]. Because the relative optical absorption contrast between blood and dermal tissue can be up to 100, depending on the optical wavelength used [6], an optical absorption-based high-resolution imaging modality is well suited for microvascular imaging. Moreover, since optical absorption is associated with both forms of hemoglobin in blood, optical absorption-based imaging can quantify functional parameters such as the total hemoglobin concentration and hemoglobin oxygen concentration (SO_2).

The ratio of the maximum imaging depth to the depth (axial) resolution, which gives the number of effective pixels, is used to evaluate the spatial resolution and image quality of an imaging modality. A depth-to-resolution ratio greater than 100 has been achieved by several optical modalities, such as confocal microscopy, two-photon microscopy, and optical coherence tomography (OCT). However, all are not directly dependent on optical absorption contrast, and none can reach a penetration depth of more than ~1 mm (related to one transport mean free path) in biological tissue owing to strong optical scattering. Hence, existing high-resolution optical imaging modalities are not ideal for imaging subcutaneous microvasculatures.

#72153 - $15.00 USD Received 20 June 2006; revised 14 August 2006; accepted 14 August 2006

Photoacoustic (PA) imaging [3,7-12] is a hybrid imaging modality based on optical absorption contrast and ultrasonic localization; it provides volumetric imaging of subcutaneous microvasculature with high spatial resolution at large depths. In PA imaging, a short laser pulse illuminates the biological tissue. When light energy is absorbed, a local temperature rise leads to a thermal-elastic expansion and, subsequently, the generation of a pressure wave (referred to as a PA wave). The PA wave is then detected to image the internal optical absorption distribution. Deeply penetrating diffuse photons can produce PA waves, and PA waves scatter two to three orders of magnitude less than light in biological tissue [6]; consequently, PA imaging can image beyond one transport mean free path with high spatial resolution. The spatial resolution of PA imaging is determined by the ultrasonic parameters [13], and, thus far, an imaging depth of 9 mm and a resolution of 10 μm [7] has been reported. Previously, three-dimensional (3D) PA images have been acquired from phantoms [7], *ex vivo* blood vessels [8], large *in vivo* human blood vessels [9], and *in vivo* animal brains [10]. However, imaging of both anatomy and functions of microvasculatures in three dimensions *in vivo* has not been reported yet.

Here, we report on *in vivo* structural and functional volumetric imaging of subcutaneous microvasculature by photoacoustic microscopy (PAM). PAM is a newly developed reflection (backward) mode confocal PA imaging technique [14,15]. Unlike the reconstruction-based PA tomography (PAT) [7,10,11], which employs an unfocused ultrasonic detector and relies on an inverse algorithm to reconstruct an image, PAM uses a focused ultrasonic detector and forms volumetric images directly. Unlike previously proposed confocal PA imaging [12], PAM uses a dark-field optical illumination and an optical focus that is much larger than the ultrasonic focus [14]. In PAM, the axial resolution is inversely related to the system bandwidth; the lateral resolution is determined by the ultrasonic focal capability. As a result, an ultrasonic transducer with a high central frequency, large bandwidth, and large NA is required for high-resolution imaging. However, ultrasonic attenuation increases with the ultrasonic frequency and limits the imaging depth. Therefore, a trade-off must be made between spatial resolution and imaging depth.

In this paper, we apply PAM to achieve volumetric imaging of (1) the anatomy of the subcutaneous microvasculature in rats, (2) the SO_2 in arterioles and venules in rats, and (3) the anatomy of the subcutaneous vasculature in humans. All experimental animal procedures were in conformity with the guidelines of the US NIH [16]. The laboratory animal and human subject protocols for this work were approved by Texas A&M University.

2. Experimental setup and image formation

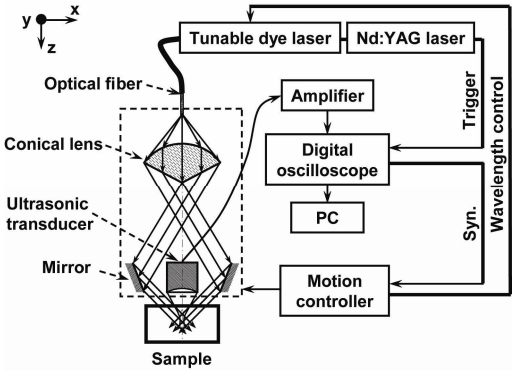

Fig. 1. Schematic of the PAM system.

A schematic diagram of the PAM is shown in Fig. 1. A tunable dye laser serves as the PA-excitation source. Laser light at a designated wavelength was delivered through an optical fiber (core diameter: 600 μm). Light was first expanded by a conical lens to form an annular beam and was then weakly focused into the tissue with its focal region coaxially overlapping

#72153 - $15.00 USD Received 20 June 2006; revised 14 August 2006; accepted 14 August 2006

the ultrasonic focus. The PA signals detected by a high-frequency focused ultrasonic transducer were amplified by a wide-band low-noise amplifier and were then digitized by an oscilloscope (sampling rate: 250 MHz). Detailed system parameters can be found in Refs. [14] and [15].

Volumetric imaging of PAM was accomplished via either raster or contour scanning. At each transducer position, the PA signal was recorded for 2 μs without signal averaging and was converted, based on the sound velocity in soft tissue (1.54 mm/μs), into a one-dimensional depth-resolved image (A-line) in the *z* direction. Mechanical translation of the optical-ultrasonic assembly within the dashed box in Fig. 1 along an *x*-*y* plane, while the *z* position was either fixed for raster scanning or dynamically adjusted for contour scanning, produced a complete 3D image.

A two-dimensional (2D) point-spread-function (PSF) of this PAM system was acquired by imaging the cross-section of a carbon fiber (diameter: 6 μm) immersed in a turbid medium. From the PSF, the axial and lateral resolutions measured 15 μm and 45 μm, respectively. The maximum imaging depth reached 3 mm [15]. Thus, the depth-to-resolution ratio is more than 100, which is comparable to that of the existing high-resolution optical modalities.

According to the current spatial resolutions, the minimum imagable vessel diameter is 20-50 μm. However, PAM can potentially resolve capillary since its spatial resolutions are scalable with the ultrasonic parameters [15].

3. Results and discussion

3.1 Structural imaging of subcutaneous microvasculatrure in rats

A Sprague-Dawley rat with a body weight of 200 g was used in this study. The dorsal side of the rat was depilated with a commercial human hair-removing lotion before data acquisition. A dose of 87 mg/kg Ketamine plus 13 mg/kg Xylasine was administered intramuscularly to anesthetize the rat. Supplemental injections of the same anesthetic mixture (~50 mg/kg/hour) minimized motion throughout the experiment. During the experiment, the body temperature was maintained; the heart rate and systemic arterial SO_2 were monitored.

In this study, the optical wavelength was 584 nm, which is one of the isosbestic points. At an isosbestic point, oxyhemoglobin (HbO_2) and deoxyhemoglobin (HbR) have an identical molar extinction coefficient; therefore, the optical absorption is dependent only on the total hemoglobin concentration and is independent of the SO_2 level. As a result, PA signals generated from venules and arterioles have comparable amplitudes.

A volume of 10×8.2×3 mm^3 was imaged at a scanning step size of 50 μm. Because the spherically focused ultrasonic detector has a focal zone of only 0.3 mm, a large portion of the imaged volume was outside the ultrasonic focal zone, where the lateral resolution was degraded. As a result, the microvessels out of the focal region could not be accurately resolved. To overcome this problem, we adopted the following two methods.

First, a contour scan was performed, in which the optical-ultrasonic assembly maintained a constant distance from the skin surface contour. Hence, good ultrasonic focusing on the subcutaneous blood vessels was ensured throughout the scanning. In preparation for a contour scan, a raster pre-scan at a constant *z* coordinate was conducted. Then the skin surface contour was extracted from the pre-scanned volumetric image. An optimal distance between the optical-ultrasonic assembly and the skin surface was chosen based on the ultrasonic focal length and the targeted mean vessel depth. In the contour scan, the *z* coordinate of the optical-ultrasonic assembly was adjusted with the *x*-*y* coordinates based on the preset optimal distance and the detected skin surface contour.

Second, a synthetic aperture focusing technique (SAFT) based on a virtual point detector concept was employed to improve the degraded out-of-focus lateral resolution [17]. In phantom tests, nearly depth-independent lateral and axial resolutions were achieved within a depth range of ±1 mm from the focal plane.

Since most vessels in the subcutaneous microvasculature of rats form a layer of less than 2 mm in thickness beneath the skin surface, combining the contour scan and the SAFT

#72153 - $15.00 USD Received 20 June 2006; revised 14 August 2006; accepted 14 August 2006

generated a well-focused volumetric image of the entire subcutaneous microvasculature as shown in Fig. 2. The laboratory *z* coordinate was recovered by shifting the moving *z* coordinate for the contour scan by the amount of the corresponding *z* coordinate of the skin surface contour. Strong PA signals generated within a 0.18-mm depth of the skin surface were digitally removed to avoid over-shadowing the rest of the image. Figure 2(A) is a maximum-amplitude-projection image (MAP), where the maximum value of the PA signal along each A-line was projected onto the *x*-*y* plane. Figure 2(B) is a volume rendering showing the vessels of various depths and orientations. The mean depth of the imaged vessels was 0.38±0.11 mm from the detected skin surface. The opacity (alpha value) and the color of each voxel were mapped according to its PA amplitude using a commercial software package (VolView, Kitware, NY).

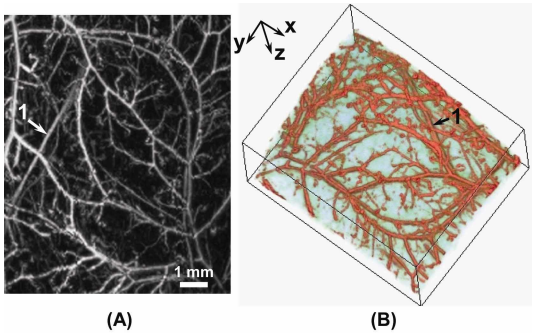

Fig 2. Structural imaging of the subcutaneous microvasculature in rats *in vivo*. (A) An MAP image. (B) (1.6 MB) A movie of the volume-rendered microvasculature viewed from different angles.

In Fig. 2(A), many vessels are less than 50 μm in diameter and thus occupy only a single pixel. The microvessel density (MVD) is approximately uniform within the whole image. The ratio of the PA amplitude of the vessels to that of the background is 19.1±5.4 on average, which demonstrates a high contrast. In Fig. 2(B), up to eight orders of vessel branching are observed. Although not revealed in the MAP image, the depth relation of the vessel numbered 1 with the major vessels above is well visualized in the movie.

For both the raster pre-scan and the contour scan, the data acquisition time totaled 130 minutes. Although the contour scan along with a raster scan takes a longer acquisition time, it is useful for applications where the skin contour varies significantly. Moreover, the pre-scan can be accelerated by enlarging the step size and then finding the skin surface contour by spline interpolation.

3.2 Imaging of SO_2 in rats in vivo

The capability of PAM to image quantitatively static SO_2 in the subcutaneous microvasculature was previously demonstrated with 2D MAP images on a vessel-by-vessel basis [15]. Here, static SO_2 in the subcutaneous microvasculature of a rat (body weight: 200 g) under hyperoxia is visualized volumetrically. The arterioles and venules are segmented and then differentiated based on their SO_2 levels (Fig. 3). With raster scanning only, the data acquisition took 160 minutes.

Based on the PA images acquired at four optical wavelengths (578, 584, 590, and 596 nm), the relative concentrations of HbO_2 and HbR (denoted by $[HbO_2]$ and [HbR], respectively) were calculated in three dimensions. The blood vessels were segmented from the structural image acquired at the 584-nm optical wavelength; then, the SO_2, defined as $[HbO_2]/([HbO_2]+[HbR])$, was calculated point-by-point only within the blood vessels. Finally, arterioles and venules were differentiated based on their physiological difference in either SO_2 or [HbR]; however, [HbR] was preferred for its robustness; specifically, the following steps were taken.

#72153 - $15.00 USD Received 20 June 2006; revised 14 August 2006; accepted 14 August 2006

First, the venules were segmented in the [HbR] image. Ideally, such a segmentation could be achieved based on simple thresholding because the [HbR] in the venules is much higher than that in the arterioles [18]. However, noise in the raw data and systematic errors in the calculation of the [HbR] [19] led to negative concentrations, bright spots in the background, and discontinuities in the vessels, which made direct thresholding ineffective. To improve the efficacy of thresholding, we set the negative concentrations in the 3D [HbR] data to zeros and then used multiscale vesselness filtering [20] to enhance equally tubular structures with various diameters in the volumetric data. After filtering, the [HbR] image presented neither bright spots in the background nor discontinued vessels. Then the concentration values were linearly normalized to the range of 0 to 1; and venules were segmented by thresholding at 0.1. After segmentation, a venule mask was created by setting all concentrations in the venules to 1/4 and all concentrations in the background 1.

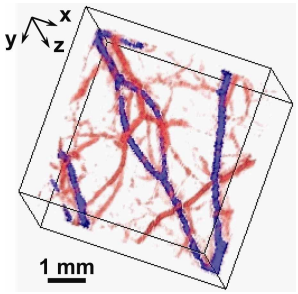

Fig. 3. (2.2 MB) A movie showing *in vivo* functional images representing SO_2 in single blood vessels of rats. Venules and arterioles are colored blue and red, respectively. The imaged average SO_2 values in the arterioles and venoules were 0.99±0.01 and 0.81±0.02, respectively.

Second, the PA amplitudes in the structural image acquired at 584 nm were linearly normalized to the range of 2^{15} to 2^{16} to introduce a bias and then multiplied by the venule mask pixelwise. The processed PA amplitudes in venules were no greater than 2^{14} and were lower than those in either the arterioles or the background in the final image. As a result, arterials and venules were divided based on the separation in the image histogram.

Finally, the venules and the arterioles were colored blue and red, respectively. The opacities of the vessels and the background were set to ~1 and less than 0.01, respectively. In Fig.3, the venules and the arterioles are at different depths, which can be observed easily in the movie.

3.3 Imaging of subcutaneous blood vessels in humans in vivo

This PAM system is considered safe for human imaging. The pulse energy was 0.2 mJ, and the energy density at the optical focus was no more than 6 mJ/cm^2 even in an optically clear medium, which is well within the ANSI safety limit in the spectral range used here (20 mJ/cm^2) [21].

Figure 4 shows a volumetric image of the subcutaneous vessels in the palm of a human hand, which was produced by an 18-minute raster scanning of 8×8 mm^2 with a step size of 80 μm. The PA signals within a depth of 0.36 mm, corresponding to the stratum corneum layer, were digitally removed. In Fig. 4, the largest vessel is approximately 350 μm in diameter and 0.7±0.07 mm beneath the skin surface.

#72153 - $15.00 USD Received 20 June 2006; revised 14 August 2006; accepted 14 August 2006

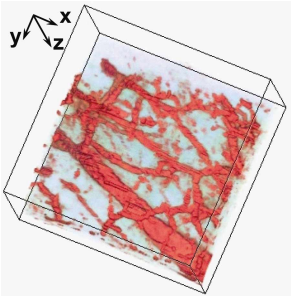

Fig. 4. Volumetric imaging of the subcutaneous blood vessels in the palm of a human hand *in vivo*.

3.4 Discussion

Volumetric PAM imaging of microvasculatures with high spatial resolution, high contrast, and high specificity *in vivo* can be invaluable for tumor angiogenesis study. In structural PAM, the MVD and the total microvascular area, which are *bona fide* predictors of aggressive tumor growth and metastases, can be calculated from MAP images. In contrast to the widely accepted dorsal flap window chamber model [22], PAM can show morphological changes of vessels in three dimensions as a tumor grows in its natural environment. In functional PAM, arterioles and venules can be individually identified in three dimensions using only intrinsic optical absorption contrast. By contrast, in magnetic resonance angiography, high-quality artery-vein identification requires the use of contrast agents [23]. As a result, PAM can provide in-depth tumor physiological studies with 3D structural and functional information of single vessels. With exogenous contrast, additional physiological functions can be measured by PAM.

Compared with 2D MAP images, volumetric visualization suffers more from motion artifacts because MAP images are insensitive to the breathing motion along the *z* axis. The major technical limitation of the current PAM setup is the low imaging speed due to the 10-Hz laser repetition rate; it, however, can be overcome by employing laser systems with high repetition rate.

4. Summary

We have shown that PAM is a new paradigm for high-quality volumetric imaging of the subcutaneous microvasculature. The anatomy of the subcutaneous microvasculature was revealed in three dimensions with high spatial resolution and high contrast in small animals and humans *in vivo*. Ultrasonic focusing on the vessel layer was maintained by a contour scan, and nearly depth-independent spatial resolution was accomplished using SAFT. SO_2 in single blood vessels was imaged in small animals on the basis of only intrinsic contrast. For the first time in PA imaging, arterioles and venules were separately identified and visualized volumetrically by means of multiscale vesselness filtering. By combining volumetric structural and functional imaging, PAM can potentially find applications in the research and early detection of superficial tumors.

Acknowledgments

We thank Dr. Geng Ku, Dr. Ovidiu Craciun, and Gina Lungu for experimental assistance. We also gratefully acknowledge the help of Dr. Yangqiu Hu in image processing. This project is sponsored by National Institutes of Health grants R01 EB000712 and R01 NS46214.

#72153 - $15.00 USD Received 20 June 2006; revised 14 August 2006; accepted 14 August 2006